Am J Physiol Heart Circ Physiol 320: H826–H837, 2021.
First published January 1, 2021; doi:10.1152/ajpheart.00608.2020

american physiological society

AMERICAN JOURNAL OF PHYSIOLOGY
HEART AND CIRCULATORY PHYSIOLOGY

RESEARCH ARTICLE

Cardiac Excitation and Contraction

The transient outward potassium current plays a key role in spiral wave breakup in ventricular tissue

Julian Landaw,[1,2] Xiaoping Yuan,[1,3] Peng-Sheng Chen,[4] and Zhilin Qu[1,2]

[1]*Department of Medicine, David Geffen School of Medicine, University of California, Los Angeles, California;* [2]*Department of Computational Medicine, David Geffen School of Medicine, University of California, Los Angeles, California;* [3]*Information Engineering School, Hangzhou Dianzi University, Hangzhou, People's Republic of China; and* [4]*Cedars-Sinai Medical Center, Los Angeles, California*

Abstract

Spiral wave reentry as a mechanism of lethal ventricular arrhythmias has been widely demonstrated in animal experiments and recordings from human hearts. It has been shown that in structurally normal hearts spiral waves are unstable, breaking up into multiple wavelets via dynamical instabilities. However, many of the second-generation action potential models give rise only to stable spiral waves, raising issues regarding the underlying mechanisms of spiral wave breakup. In this study, we carried out computer simulations of two-dimensional homogeneous tissues using five ventricular action potential models. We show that the transient outward potassium current (I_{to}), although it is not required, plays a key role in promoting spiral wave breakup in all five models. As the maximum conductance of I_{to} increases, it first promotes spiral wave breakup and then stabilizes the spiral waves. In the absence of I_{to}, speeding up the L-type calcium kinetics can prevent spiral wave breakup, however, with the same speedup kinetics, spiral wave breakup can be promoted by increasing I_{to}. Increasing I_{to} promotes single-cell dynamical instabilities, including action potential duration alternans and chaos, and increasing I_{to} further suppresses these action potential dynamics. These cellular properties agree with the observation that increasing I_{to} first promotes spiral wave breakup and then stabilizes spiral waves in tissue. Implications of our observations to spiral wave dynamics in the real hearts and action potential model improvements are discussed.

NEW & NOTEWORTHY Spiral wave breakup manifesting as multiple wavelets is a mechanism of ventricular fibrillation. It has been known that spiral wave breakup in cardiac tissue can be caused by a steeply sloped action potential duration restitution curve, a property mainly determined by the recovery of L-type calcium current. Here, we show that the transient outward potassium current (I_{to}) is another current that plays a key role in spiral wave breakup, that is, spiral waves can be stable for low and high maximum I_{to} conductance but breakup occurs for intermediate maximum I_{to} conductance. Since I_{to} is present in normal hearts of many species and required for Brugada syndrome, it may play an important role in the spiral wave stability and arrhythmogenesis under both normal condition and Brugada syndrome.

action potential model; spiral wave breakup; transient outward potassium current; ventricular arrhythmias

INTRODUCTION

The leading cause of sudden cardiac death (SCD) is ventricular arrhythmias (1), in which focal excitations and reentry are the main abnormal electrical activities in the ventricular muscle of the heart (2, 3). Although the exact forms of electrical dynamics responsible for ventricular arrhythmias are still debatable (4–7), spiral waves (also called "rotors") as a form of functional reentry have been widely demonstrated in experiments of animal hearts (8–21) and recordings from human hearts (22–24). In most of the cases, ventricular arrhythmias manifest as multiple spiral waves or rotors. Moreover, the number of spiral waves does not remain constant but is highly variable over time (8, 14, 25). Because of this spatiotemporal irregularity in spiral wave dynamics, the resulting pseudo-ECG is also highly irregular. In clinical settings, polymorphic ventricular tachycardia (VT) and ventricular fibrillation (VF), two dangerous forms of arrhythmia, also exhibit irregular ECGs. This indicates that unstable spatiotemporal spiral wave dynamics may indeed be responsible for these lethal forms of human ventricular arrhythmias.

It is well known that complex spatiotemporal spiral wave dynamics can be caused by either tissue heterogeneities or

Correspondence: Z. Qu (zqu@mednet.ucla.edu).
Submitted 23 July 2020 / Revised 22 December 2020 / Accepted 22 December 2020

by voltage or calcium (Ca^{2+})-driven dynamical instabilities, or interactions of both (2, 26). In early computer simulations using simple action potential (AP) models, such as the Noble model (27, 28), the Beeler–Reuter model (29–32), the 1991 Luo–Rudy (LR1) model (33), and other simplified AP models (34–37), it has been shown that the slope of the AP duration (APD) restitution curve is a major parameter determining spiral wave stability. One can change the slope of the APD restitution curve and thus the spiral wave stability by adjusting the maximum conductance of some ionic currents, in particular the maximum conductance of the L-type calcium (Ca^{2+}) current ($I_{Ca,L}$) or the potassium (K^+) currents (33, 38). The roles of APD restitution in spiral wave stability have also been demonstrated in many experiments (10, 39–43). However, more recent computer simulations (44–47) have shown that many of the second-generation physiologically detailed AP models (48–52) give rise to stable spiral waves in tissue, whereas only a few of them (53–55) result in unstable spiral wave dynamics. The major reason that the spiral waves are stable in these models is that the slopes of the APD restitution curves are small (46), which may be a result of the much faster kinetics of $I_{Ca,L}$ in the second-generation AP models (49). Note that these AP models were developed based on experimental data from ventricular myocytes of normal hearts. The fact that the spiral waves are stable in tissue with the myocytes described by these AP models disagrees with the observation that spiral waves are highly variable and short-lived during ventricular arrhythmias in normal hearts.

In this study, we seek to investigate spiral wave stability in tissues with the electrophysiological behaviors of the myocytes described by the second-generation AP models. We hypothesize that the transient outward K^+ current (I_{to}) is a key current promoting spiral wave instability in cardiac tissue. The rationale for this hypothesis is that it has been widely shown that I_{to} can promote dynamical instabilities resulting in complex APD dynamics in cardiac myocytes (56–59). These cellular instabilities may also promote spiral wave instabilities in the tissue scale to result in spiral wave breakup. I_{to} is primarily present in the right ventricle and the epicardial layer of left ventricle (59–61). Moreover, I_{to} is a current required for J-wave syndrome and Brugada syndrome (62, 63), which can give rise to phase-2 reentry (64, 65). Therefore, the objectives of this study are twofold: *1*) to understand the role of I_{to} in promoting spiral wave instabilities and thus its role in arrhythmogenesis in J-wave syndrome and Brugada syndrome, and *2*) to examine if spiral wave breakup can be promoted in the second-generation AP models by increasing the maximum I_{to} conductance (G_{to}). We carry out simulations of two-dimensional (2-D) homogeneous tissue models using several widely used second-generation ventricular AP models. We show that spiral wave breakup is promoted by increasing G_{to}; however, the spiral waves become stable when G_{to} is large enough. To better understand the underlying mechanisms by which I_{to} promotes spiral wave breakup, we carry out simulations using the simple LR1 model. We show that in the absence of I_{to}, speeding up the $I_{Ca,L}$ kinetics (one of the major improvements made in the second-generation AP models) stabilizes spiral waves, but spiral wave breakup can still be promoted by increasing the maximum conductance of I_{to}. Implications of our observations to spiral wave dynamics in the real heart and improvements of the AP models are discussed.

METHODS

Mathematical Models

We carried out single-cell and two-dimensional (2-D) tissue simulations with different ventricular myocyte AP models. The differential equation for voltage for single-cell simulations is as follows:

$$\frac{dV}{dt} = (-I_{ion} + I_{sti})/C_m, \quad (1)$$

where C_m = 1 μF/cm^2 is the membrane capacitance, I_{ion} the ionic current density, and I_{sti} the external stimulus current density. The differential equation for voltage of 2-D tissue is as follows:

$$\frac{\partial V}{\partial t} = -\frac{I_{ion}}{C_m} + D\left(\frac{\partial^2 V}{\partial x^2} + \frac{\partial^2 V}{\partial y^2}\right), \quad (2)$$

where D is the diffusion constant. We used the following AP models: *1*) the 1991 Luo and Rudy (LR1) guinea pig ventricular AP model (66); *2*) the 1994 Luo and Rudy (LRd) guinea pig ventricular AP model with later modifications (49, 67); *3*) the Mahajan et al. rabbit ventricular AP model (68); *4*) the O'Hara et al. (ORd) human ventricular AP model (50); and *4*) the 2004 ten Tusscher et al. (TP04) human ventricular AP model (52). Except for the LR1 model, computer codes of the single-cell AP models were downloaded from the websites of the original authors to ensure originality of the models. These single-cell models were implemented in 2-D tissue using *Eq. 2*. We used D = 0.00154 cm^2/ms for the TP04 model, the original value used by ten Tusscher et al. (52). We used D = 0.001 cm^2/ms for the other models, which gives rise to a conduction velocity around 0.55 m/s for the LR1 model with a maximum I_{Na} conductance of 16 mS/cm^2 (38). No-flux boundary conditions were used.

Simulation Methods

We used the typical cross-field protocol to induce a single spiral wave in the 2-D tissue. The initial conditions were set as follows. A single cell (*Eq. 1*) was paced at a pacing cycle length (PCL) of 500 ms for 1,000 beats to remove transient behaviors. The values of all the variables were recorded at the end of the pacing and they were used as the initial conditions for all the cells in the 2-D tissue. The entire left boundary of cells in the tissue was then paced, triggering a wave propagating toward the center of the tissue. Once the propagated wave repolarizes at the center of the tissue, all cells in the bottom half of the tissue were depolarized by fixing their voltages to −30 mV for 2 ms. Afterward, *Eq. 2* was integrated for 5–10 s. APD and the spiral wave cycle length (CL) were calculated from a cell located at (3.2 cm, 3.2 cm) in the tissue. APD was defined as the time period in which V remains above −75 mV.

For all the models, the 2-D tissue was discretized as $\Delta x = \Delta y$ = 0.0125 cm, with 2,048 × 2,048 discretized cells for all models except for the LR1 model. A 1,024 × 1,024 cells were used for the LR1 model. A time-adaptive forward Euler method was used with a time step of Δt = 0.0025 ms if the

change in voltage $\Delta V > 0.1$ mV in a time step, otherwise the time step is $\Delta t = 0.025$ ms. Simulations were performed on Tesla and GeForce GPUs (NVIDIA corporation) using C++ programs in CUDA, a programming language designed for graphical processing units.

RESULTS

I_{to} Promotes Spiral Wave Breakup in Tissue Using the LRd Model

The LRd model is an AP model for guinea pig ventricular myocytes developed in 1994 by Luo and Rudy (49); in this study, we used the later modified version by Faber and Rudy (67) with an I_{to} formulation given by Gima and Rudy (69). We first simulated spiral wave dynamics in the LRd model with different G_{to}. A spiral wave in 2-D tissue using the original LRd model is stable with small variations in CL and APD (Fig. 1*A*). In this case, the maximum I_{to} conductance is G_{to} = 0.5 mS/cm^2 which was set as the control value. When G_{to} is two times of the control value (Fig. 1*B*), spiral wave breakup occurs with CL and APD varying in large ranges and irregularly. When G_{to} is five times of the control value (Fig. 1*C*), spiral wave breakup still occurs but the wavelength becomes apparently shorter. APD remains below 40 ms and CL around 60 ms but can be occasionally large (APD ~100 ms and CL ~150 ms). When G_{to} is 6.5 times of the control value, spiral wave breakup occurs initially with large CL but small APD variations. The CL and APD eventually become unchanged (Fig. 1*D*). In this case, after the initial chaotic spiral wave breakup phase, the spiral waves become stable, and thus the spiral wave pattern, although spatially irregular, is temporally periodic. When G_{to} is 10 times of the control value (Fig. 1*E*), no breakup occurs, and the spiral wave is completely stable with a much shorter APD and CL compared with control. We replotted the values of APD and CL from the aforementioned cases in a single panel (Fig. 1*F*) to compare the APD and CL variations.

We systematically explored the spiral wave behaviors for different maximum $I_{Ca,L}$ conductance (P_{Ca}, which was used in the AP models to describe the strength of $I_{Ca,L}$, proportional to the maximum conductance) and G_{to} while maintaining other parameters at their control values, summarized in Fig. 1*G*. We used the cross-field protocol

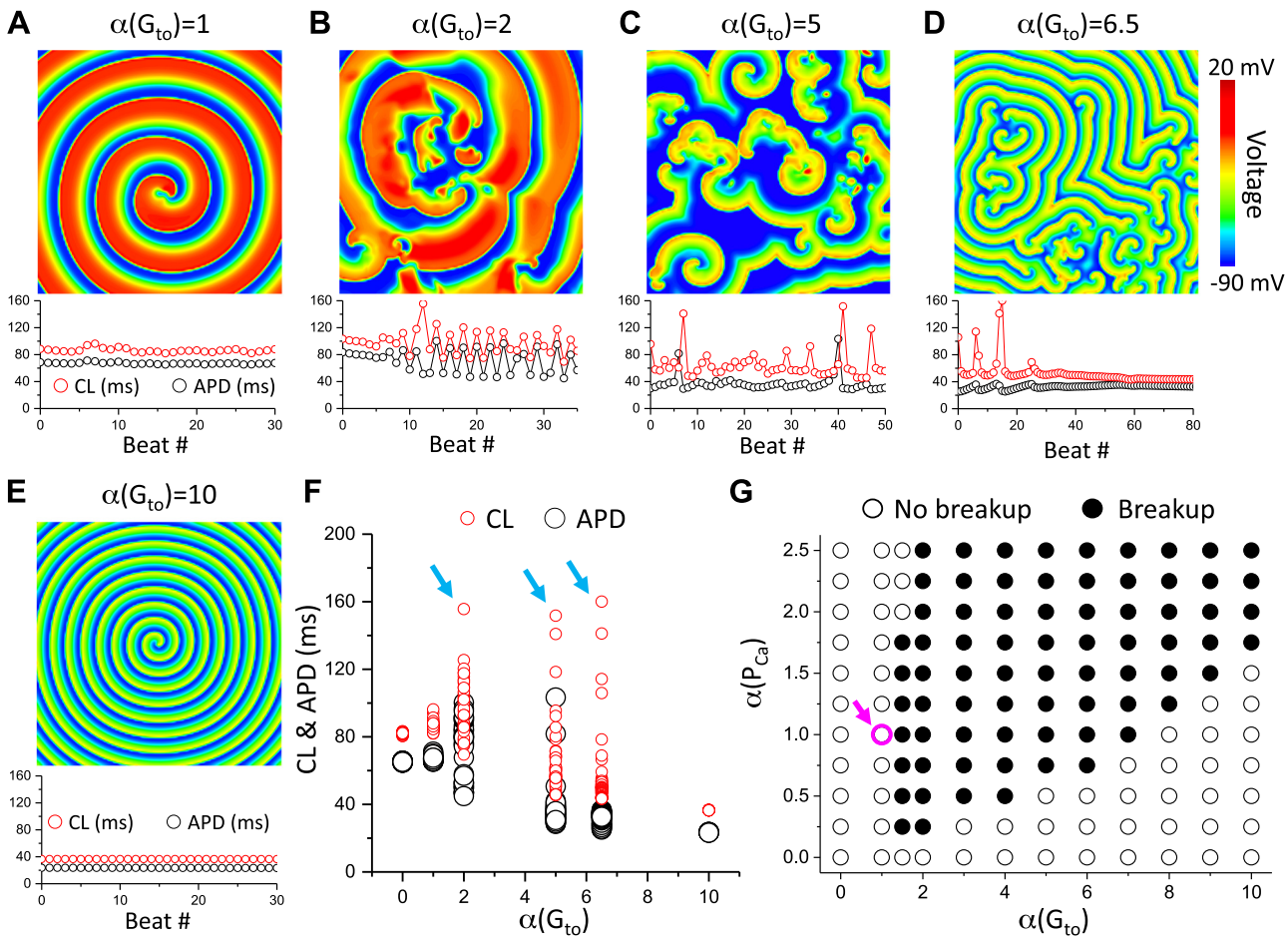

Figure 1. Effects of the maximum I_{to} conductance on spiral wave breakup in two-dimensional (2-D) tissue with the 1994 Luo and Rudy (LRd) model. *A–E*: voltage snapshots (*upper*) and CL and APD vs. beat # (*lower*) for the original (control) LRd model (*A*), two times of the control G_{to} (*B*), five times of the control G_{to} (*C*), 6.5 times of the control G_{to} (*D*), and 10 times of the control G_{to} (*E*). *F*: APD and CL vs. $\alpha(G_{to})$ replotted from data shown in *A–E*. Cyan arrows indicate the G_{to} with spiral wave breakup. *G*: spiral wave behaviors versus $\alpha(P_{Ca})$ and $\alpha(G_{to})$. The magenta circle and arrow mark the parameter set of the original LRd model (control). The control G_{to} is 0.5 mS/cm^2.

AJP-Heart Circ Physiol • doi:10.1152/ajpheart.00608.2020 • www.ajpheart.org

described in METHODS to induce a single spiral wave in the tissue. If this spiral wave remained intact without breakup, we labeled the point as "no breakup" (open circles). If the spiral wave did not remain intact, but degenerated into multiple spiral waves, whether they finally became stable (such as the case in Fig. 1*D*) or unstable (such as the cases in Fig. 1, *B* and *C*), we labeled the point as "breakup" (solid circles). As shown in Fig. 1*G*, spiral wave breakup occurs in a wide range of parameters when I_{to} is present. When I_{to} is absent (G_{to} = 0) or at its control value, no spiral wave breakup occurs for P_{Ca} ranging from 0 to 2.5 times of its control value. When G_{to} is larger than its control value, spiral wave breakup occurs in a wide range of P_{Ca}. When G_{to} is too large, the spiral wave becomes stable again. Note that at the left boundary from no breakup to breakup, a larger P_{Ca} prevents breakup (see the third column from the left). At the right boundary from breakup to no breakup, a larger P_{Ca} promotes breakup.

As shown in Fig. 1, I_{to} plays a critical role in spiral wave breakup in the LRd model. We then test whether spiral wave breakup can occur in the LRd model in the absence of I_{to}. We set G_{to} = 0 and varied the maximum conductance of other ionic currents to assess the spiral wave dynamics. Figure 2 plots APD and CL for different fold changes of the maximum conductance of $I_{Ca,L}$ (Fig. 2*A*), I_{Kr} (Fig. 2*B*), I_{Ks} (Fig. 2*C*), and I_{K1} (Fig. 2*D*). We did not observe spiral wave breakup for P_{Ca} from 0 to 2.75 times of its control value, for G_{Kr} from 0 to 5 times of its control value, for G_{Ks} from 0.5 to 5 times of its control value, or for G_{K1} from 0.5 to 2 times of its control value. However, when G_{K1} is larger than 2.5 times of its control value, spiral wave breakup occurs (indicated by arrows in Fig. 2*D*). Therefore, in the LRd model and in the absence of I_{to}, no spiral wave breakup can occur in wide ranges of parameters away from their control values.

To gain some insights into I_{to} promoting APD instabilities in the LRd model, we carried out single-cell simulations. Figure 3*A* shows a bifurcation diagram showing APD versus G_{to} for PCL = 500 ms. When G_{to} is small, APD is stable, that is, APD is the same from beat to beat. As G_{to} is increased to certain value, APD instabilities occur, in which APD changes from beat to beat, such as APD alternans and chaos. As G_{to} increases further, APD becomes stable again but becomes much shorter. Figure 3*B* shows the APD behaviors for different PCL and G_{to}. For the control G_{to} [$\alpha(G_{to})$ = 1], APD is stable for any PCL, which agrees with the observation that there is no spiral wave breakup in the control LRd model. For very large G_{to}, APD becomes stable again, which also agrees with the observation that spiral wave is stable when I_{to} conductance is large enough.

I_{to} Promotes Spiral Wave Breakup in Tissue Using Other Ventricular AP Models

We carried out simulations in 2-D tissue using three other AP models for spiral wave stability: the rabbit ventricular myocyte model by Mahajan et al. (68), the TP04 human ventricular myocyte model (52), and the ORd human ventricular myocyte model (50). For each model, we showed voltage snapshots for G_{to} = 0, control G_{to}, an intermediate G_{to} causing spiral wave breakup, and a very large G_{to} resulting in a stable spiral wave. We also investigated spiral wave stability in the absence of I_{to} by varying the maximum conductance of other currents.

Figure 4 shows the results for the Mahajan et al. model. We varied the maximum conductance of the fast I_{to} ($I_{to,f}$) in this model. The spiral wave is stable for G_{to} = 0 and the control G_{to} (0.11 mS/cm^2), breaks up when G_{to} is two times of its control value, and becomes stable when G_{to} is four times of its control value (in Fig. 4*A*, *left*). The *right* panel plots APD and CL for the four cases, which show when spiral wave breakup occurs, both APD and CL varied in wide ranges. In the absence of I_{to} (Fig. 4*B*), spiral wave breakup occurs when

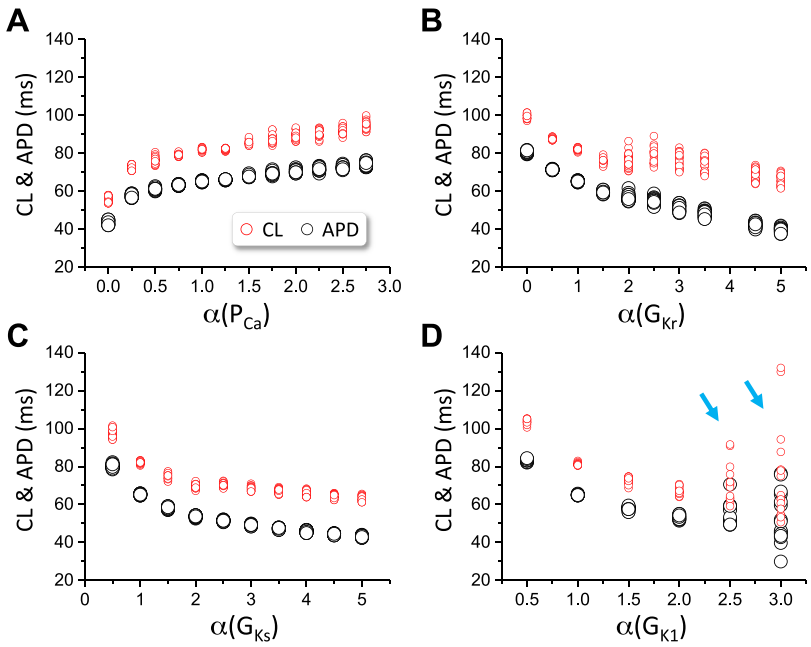

Figure 2. Spiral wave dynamics in two-dimensional (2-D) tissue with the Luo and Rudy (LRd) model in the absence of I_{to}. cycle length (CL) and action potential duration (APD) of spiral waves vs. the fold change (α) of the maximum conductance of different ionic currents. G_{to}=0. The 2-D tissue simulations were done the same way as in Fig. 1. *A*: P_{Ca}. *B*: G_{Kr}. *C*: G_{Ks}. *D*: G_{K1}. Cyan arrows indicate that breakup occurs.

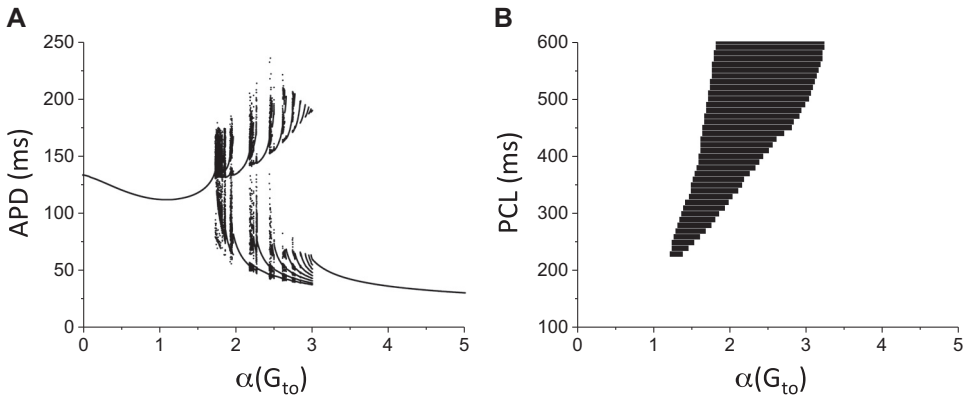

Figure 3. Effects of I_{to} on action potential duration (APD) dynamics in a single Luo and Rudy (LRd) cell. *A*: bifurcation diagram showing APD vs. $\alpha(G_{to})$ for pacing cycle length (PCL) = 500 ms. For each $\alpha(G_{to})$ value, 100 APDs were plotted. *B*: region of APD instability for different G_{to} and PCL. The black region is the unstable region in which APD varies from beat to beat, including APD alternans and chaos.

P_{Ca} is 1.5 times its control value or larger or when G_{Ks} is reduced by half. Therefore, I_{to} promotes spiral breakup but is not required in this model.

Figure 5 shows the results for the TP04 model. The spiral wave is stable for G_{to} = 0 and control G_{to} (0.294 mS/cm^2), breaks up when G_{to} is 20 times of its control value, and becomes stable when G_{to} is 100 times of its control value (in Fig. 5*A*, *left*). APD and CL vary in wide ranges when spiral breakup occurs (in Fig. 5*A*, *right*). However, in the absence of I_{to}, no spiral wave breakup occurs in this model when the maximum conductance of the selected ionic currents is doubled or halved (Fig. 5*B*).

We observed the same spiral wave behaviors for the ORd model (Fig. 6). That is, the spiral wave is stable for G_{to} = 0 and control G_{to} (0.08 mS/cm^2), breaks up in intermediate G_{to}, and becomes stable when G_{to} is very large. In the absence of I_{to}, no breakup occurs when the maximum conductance of other currents is doubled or halved.

L-type Ca^{2+} Channel Kinetics and I_{to} Conductance on Spiral Wave Breakup: Insights from the Simple LR1 Model

As shown in the simulation results above, I_{to} plays a critical role in spiral wave stability. In particular, for the LRd model, the spiral wave remains stable for a wide range of parameters when I_{to} is absent. One of the major changes of the LRd model from the previous models, such as the LR1 model (66) and the Beeler–Reuter model (70), was the reformulation of $I_{Ca,L}$ based on patch clamp experimental data that show much faster kinetics (49). It has been widely shown that $I_{Ca,L}$ and its kinetics play a key role in spiral wave stability (29, 30, 33, 38, 71, 72), the reformulation of $I_{Ca,L}$ is the

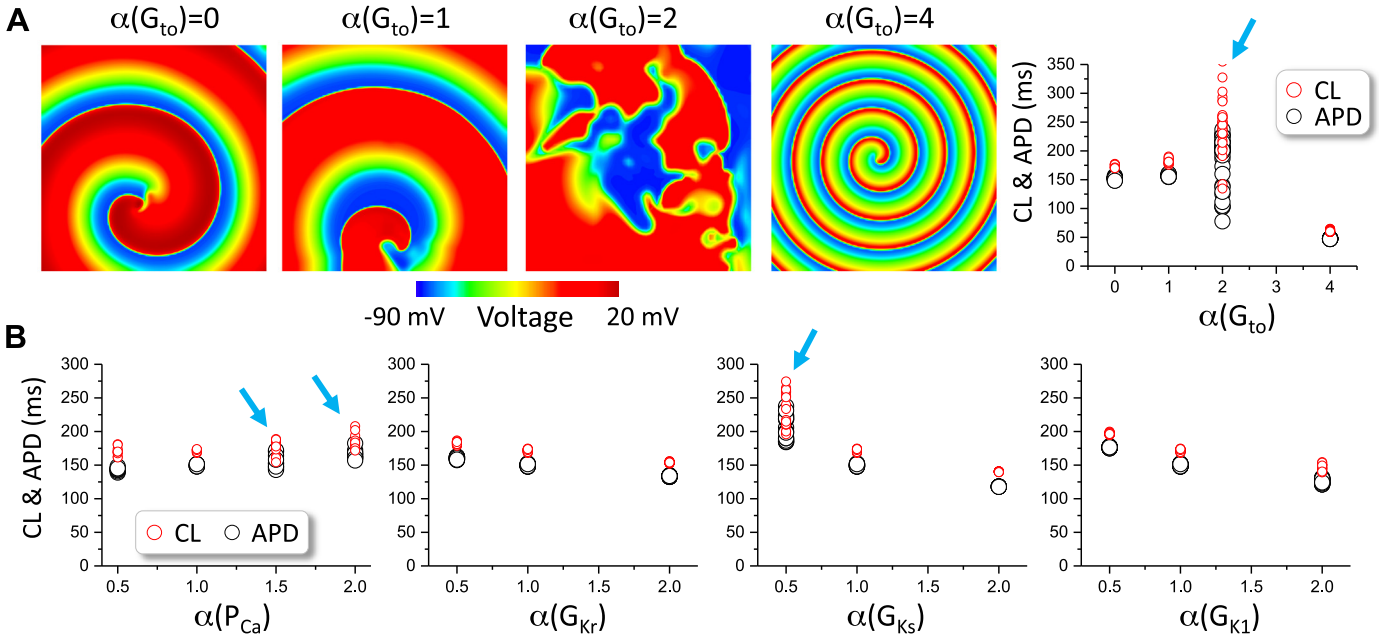

Figure 4. Spiral wave dynamics in two-dimensional (2-D) tissue with the Mahajan et al. model. *A*: *left four panels*: voltage snapshots of spiral waves at different G_{to} levels. *Right panel*: action potential duration (APD) and cycle length (CL) vs. G_{to} for the four G_{to} levels. *B*: APD and CL vs. the fold change (α) of the control maximum conductance of $I_{Ca,L}$, I_{Kr}, I_{Ks}, and I_{K1} in the absence of I_{to} (G_{to} = 0). Arrows indicate the cases of spiral wave breakup. The control G_{to} is 0.11 mS/cm^2. Only the fast component ($I_{to,f}$) was altered.

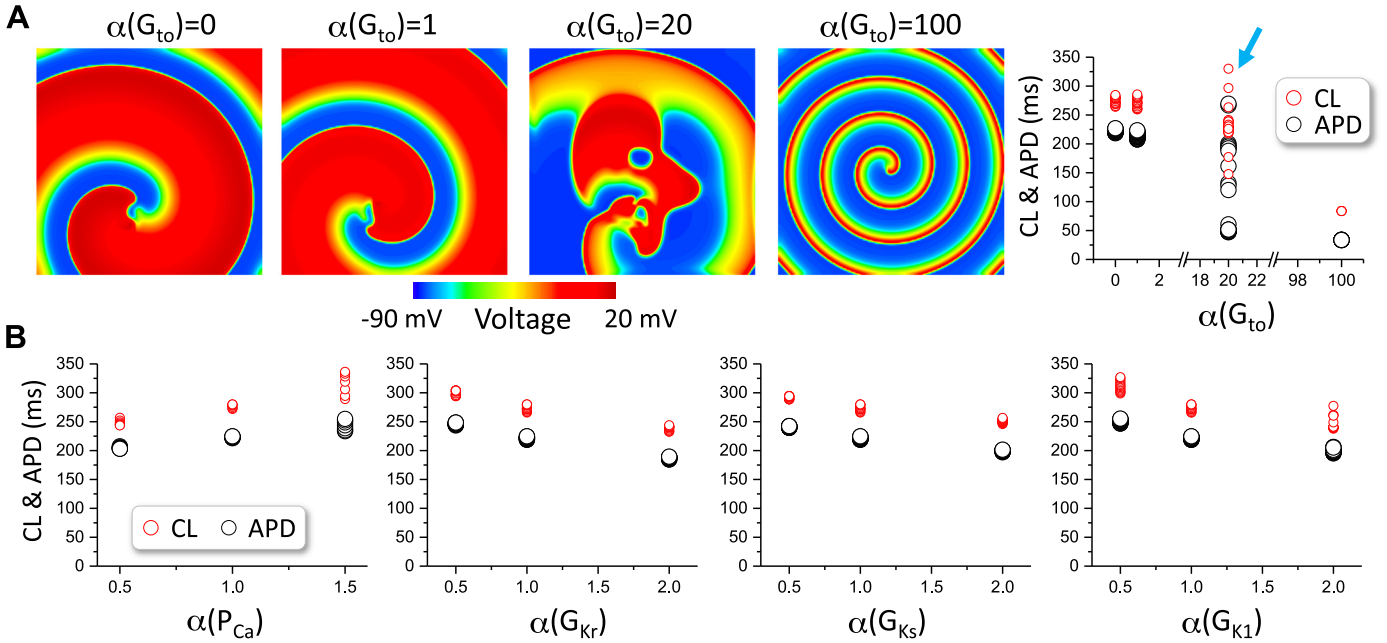

Figure 5. Spiral wave stability in two-dimensional (2-D) tissue with the TP04 model. *A*: *left four panels*: voltage snapshots of spiral waves at different G_{to} levels. *Right panel*: action potential duration (APD) and cycle length (CL) vs. G_{to} for the four G_{to} levels. *B*: APD and CL vs. the fold change (α) of the control maximum conductance of $I_{Ca,L}$, I_{Kr}, I_{Ks}, and I_{K1} in the absence of I_{to} (G_{to} = 0). Arrows indicate the cases of spiral wave breakup. The control G_{to} is 0.294 mS/cm^2. TP04, 2004 ten Tusscher et al.

most likely cause for stable spiral wave in the LRd model and other second-generation AP models. As shown in our simulations, altering other currents cannot cause spiral wave breakup (except the Mahajan et al. model) but increases in I_{to} can promote spiral wave breakup in all the AP models. Furthermore, the spiral wave becomes stable when I_{to} is very large. However, the underlying mechanism is not well understood. To gain more mechanistic insights into the effects of I_{to} on promoting spiral wave breakup, we used a relatively simple AP model, the LR1 model, to investigate the interactions of $I_{Ca,L}$ and I_{to}. We added an I_{to} [$I_{to,f}$ from the Mahajan et al. model (68)] to the model. As shown in many

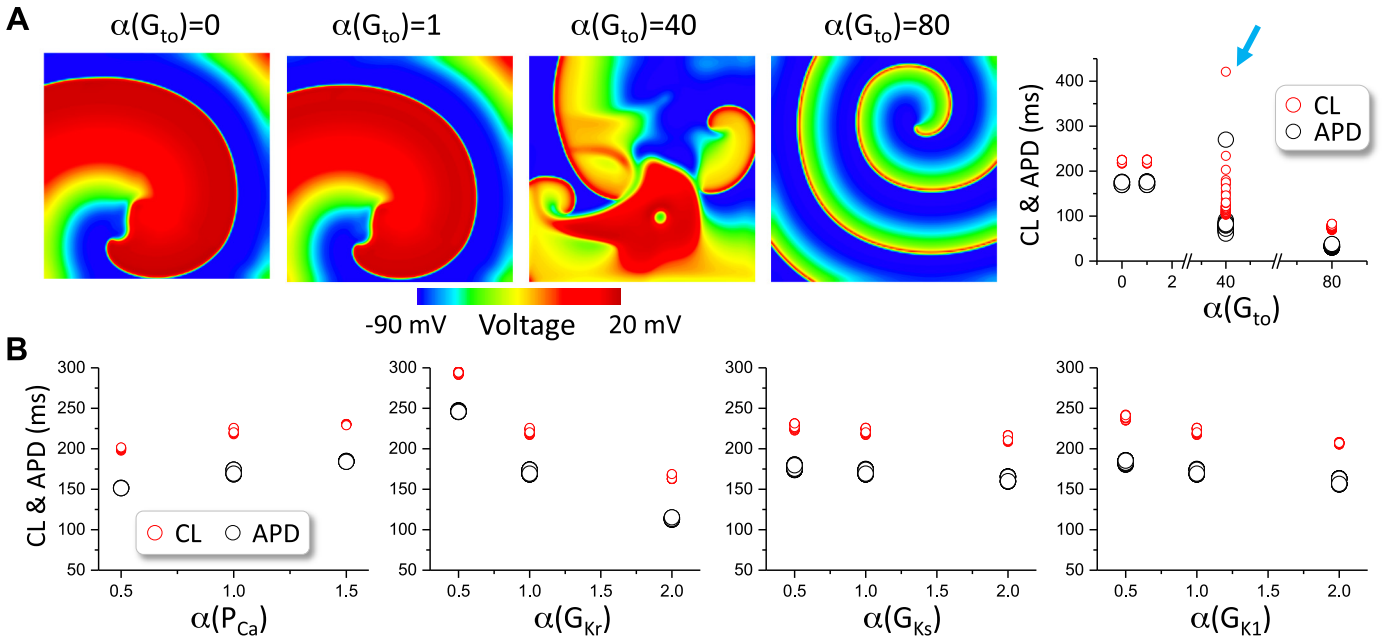

Figure 6. Spiral wave stability in two-dimensional (2-D) tissue with the O'Hara et al. (ORd) model. *A*: *left four panels*: voltage snapshots of spiral waves at different G_{to} levels. *Right panel*: action potential duration (APD) and cycle length (CL) vs. G_{to} for the four G_{to} levels. *B*: APD and CL vs. the fold change (α) of the control maximum conductance of $I_{Ca,L}$, I_{Kr}, I_{Ks}, and I_{K1} in the absence of I_{to} (G_{to} = 0). Arrows indicate the cases of spiral wave breakup. The control G_{to} is 0.08 mS/cm^2.

previous studies (33, 47, 73), spiral waves in 2-D tissue with cells described by the LR1 model are unstable. In the LR1 model, $I_{Ca,L}$ was called slow inward current (I_{si}) because of the slow kinetics adopted from the Beeler–Reuter model (70). Previous studies (29, 38, 72) have shown that speeding up the kinetics of I_{si} in the Beeler–Reuter model or the LR1 model, flattens APD restitution and stabilizes the spiral waves. We simulated two cases: the original slow I_{si} kinetics and a speedup I_{si} kinetics (70% reduction of both the activation and inactivation time constants).

In the case of the original I_{si} kinetics (Fig. 7*A*), spiral wave breakup occurs in the original model, but breakup is prevented by reducing G_{si} and/or increasing G_{to} (the *lower right* region). In the case of the speedup I_{si} kinetics (Fig. 7*B*), spiral waves are stable when G_{si} is large and G_{to} is small. As G_{to} increases, spiral wave breakup occurs. When G_{to} is even larger, spiral wave becomes stable again. Representative voltage snapshots from these three regions are shown in Fig. 7*C*. This behavior is very similar to that of the LRd model (compare Fig. 7*B* with Fig. 1*G*).

To gain more mechanistic insights into the effects of I_{to} on spiral wave stability in the LR1 model, we carried out single-cell simulations to investigate the effects of I_{to} on AP dynamics. Speeding up the I_{si} kinetics results in a flattened APD restitution curve (Fig. 8, *A* and *B*), agreeing with the fact that speeding up the I_{si} kinetics stabilizes the spiral wave. For the control kinetics, when G_{to} = 0, complex APD dynamics occurs at very fast pacing (Fig. 8*C*). As G_{to} increases, APD instabilities occur at longer PCL. As G_{to} increases further, APD become stable at short PCLs. This agrees with the observation that spiral wave becomes stable as the maximum conductance of I_{to} increases (note that the CL of spiral waves corresponds to the short PCL range). For the speedup kinetics, when G_{to} = 0, the APD is stable for all PCLs (Fig. 8*D*). However, as G_{to} increases to a certain level, unstable APD dynamics can be observed, indicating that I_{to} promoted dynamical instabilities. As G_{to} increases even further the APD become stable again. This agrees with the observation that spiral wave breakup occurs in the intermediate range of G_{to} in the case of speedup I_{si} kinetics.

DISCUSSION

In this study, we carried out simulations to investigate the roles of I_{to} in spiral wave dynamics in 2-D cardiac tissue. We simulated five ventricular AP models and investigated the spiral wave stability of each model by varying the maximum conductance of I_{to} and those of other major ionic currents. Our major finding is that the maximum I_{to} conductance and the $I_{Ca,L}$ kinetics are the two key parameters for spiral wave breakup in cardiac tissue. In this study, we discuss the mechanisms of spiral wave breakup and the mechanisms by which I_{to} promotes spiral wave breakup.

Mechanisms of Spiral Wave Breakup and the Role of $I_{ca,L}$ Recovery

Different mechanisms of spiral wave breakup in cardiac tissue have been proposed (21, 27, 33, 35, 36, 73), including: *1*) dynamical instabilities; *2*) fibrillatory conduction block caused by repolarization heterogeneities; and *3*) low and heterogeneous excitability. Note that repolarization or excitability heterogeneities are required for the latter two mechanisms but not for the first mechanism. Spiral wave breakup caused by dynamical instabilities can occur in homogeneous

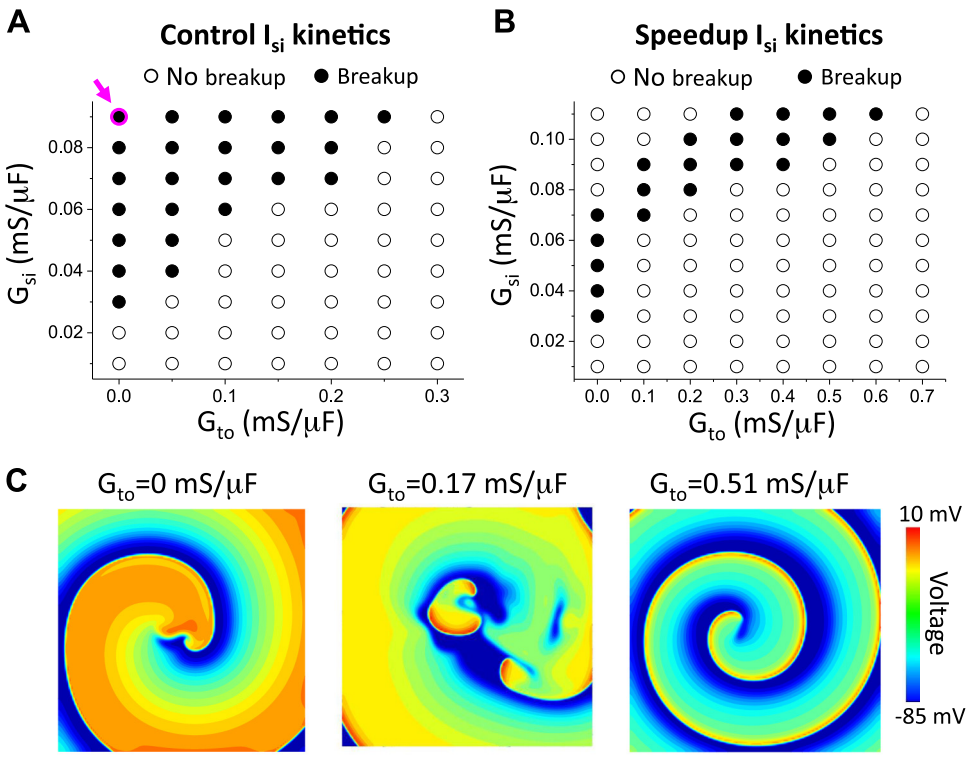

Figure 7. Spiral wave dynamics in two-dimensional (2-D) tissue with the 1991 Luo and Rudy (LR1) model. *A*: spiral wave behaviors vs. G_{si} and G_{to} with the original I_{si} kinetic. The magenta circle and arrow mark the parameter set of the original LR1 model (control). *B*: spiral wave behaviors vs. G_{si} and G_{to} for a speedup I_{si} kinetics. To speed up the kinetics of I_{si}, the time constants of the activation and inactivation gates were reduced by multiplying a factor 0.3, i.e., $\tau_d \rightarrow 0.3\tau_d$ and $\tau_f \rightarrow 0.3\tau_f$. *C*: voltage snapshots showing spiral waves for the speedup I_{si} kinetics for G_{si} = 0.09 mS/μF and different G_{to} as indicated on each panel.

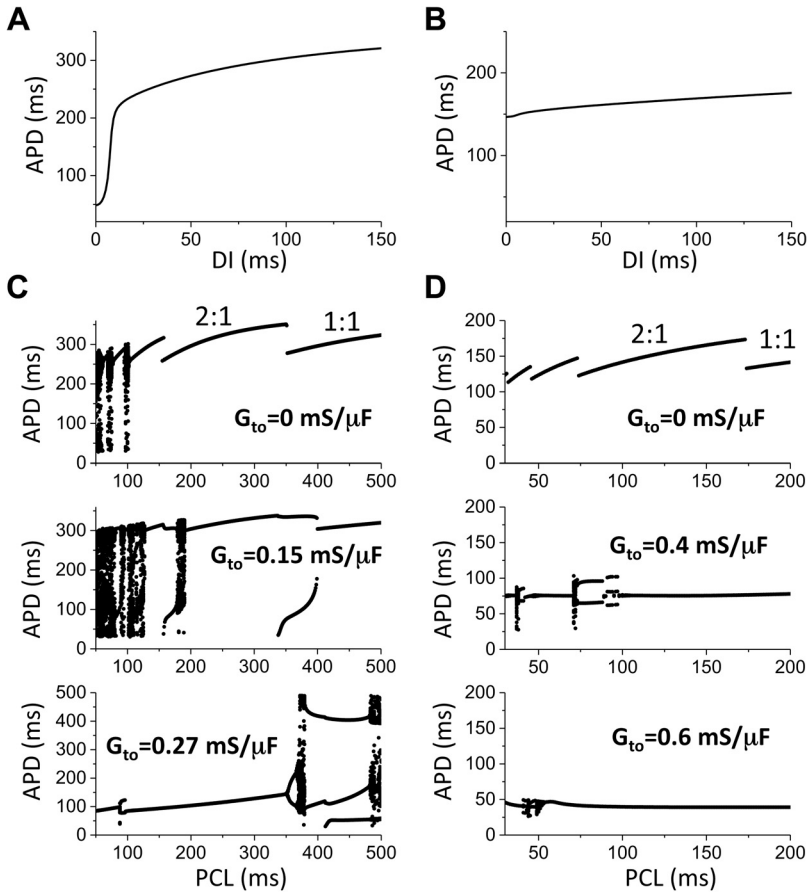

Figure 8. Effects of I_{to} on action potential duration (APD) dynamics in the 1991 Luo and Rudy (LR1) model. *A*: APD restitution curve for the control I_{si} kinetics. *B*: APD restitution curve for the speedup I_{si} kinetics. *C*: bifurcations showing APD vs pacing cycle length (PCL) for G_{to} values marked on each panel for the control I_{si} kinetics. *D*: bifurcations showing APD vs. PCL for G_{to} values marked on each panel for the speedup I_{si} kinetics.

tissue, and a steep slope of the APD restitution curve is well-known to promote dynamical instabilities. Spiral wave breakup occurs when the slope is greater than one in a wide diastolic interval (DI) range (38). The roles of APD restitution in spiral wave stability have also been demonstrated in many experiments (10, 39–43). APD restitution results from the incomplete recovery of ion channels. Although changing the conductance and kinetics of any of the currents affects APD as well as APD restitution, different currents exhibit different effects, making the effects of some currents more profound compared with others in spiral wave stability. For example, the Na^+ channel recovers quickly, and incomplete recovery of the Na^+ current at very short DIs shortens APD, contributing to the steepness of the APD restitution curve at very short DIs. Therefore, the Na^+ channel plays a very important role in spiral wave meandering (38). The L-type Ca^{2+} channels recover more slowly than the Na^+ channels, and thus affect APD restitution at longer DIs compared with that of Na^+ channels. Because of this, $I_{Ca,L}$ recovery plays a key role in spiral wave breakup (33, 38, 71). K^+ channels recover in a wide range of DIs and thus affect the APD restitution at a wide range of DIs, which also affect spiral wave stabilities.

$I_{Ca,L}$ was first formulated by Beeler and Reuter (70) and adopted in the LR1 model (66). However, the kinetics of this formulation is slow, and thus the current was called the slow-inward current (I_{si}). A major reason for the development of the LRd model (49) is to reformulate $I_{Ca,L}$ based on single-cell and single-channel experiments, which show much faster activation and inactivation kinetics. Similar $I_{Ca,L}$ kinetics were implemented in other second-generation AP models. Speeding up the kinetics flattens the APD restitution curve (Fig. 8) and thus prevents spiral wave breakup (see Fig. 7). For the same reason, the spiral wave in the LRd model is stable. As shown by Elshrif and Cherry (46), the slopes of the APD restitution curves are small in many of the second-generation AP models, which are likely caused by the fast $I_{Ca,L}$ kinetics and the major cause for stable spiral waves for these models (44–47) (also see Figs. 5 and 6).

On the other hand, in the Mahajan et al. model (68) which uses a Markovian formulation to model the proper recovery kinetics of $I_{Ca,L}$, spiral wave breakup can occur by increasing the maximum conductance of $I_{Ca,L}$ or reducing the maximum conductance of the K^+ currents (see Fig. 4). It has been shown that spiral waves are unstable and break up in tissues using the canine ventricular AP model by Hund and Rudy (44). $I_{Ca,L}$ in the Hund and Rudy model (53) was reformulated to result in a slower recovery by introducing a new gating variable with a slower time constant. $I_{Ca,L}$ was also reformulated in the 2006 version of the ten Tusscher et al. model (55) to slow the recovery, which can then exhibit APD alternans and spiral wave breakup. These modeling studies further demonstrate that the kinetics of $I_{Ca,L}$ recovery plays a

key role in promoting dynamical instabilities for spiral wave breakup.

Mechanism by Which I_{to} Promotes Spiral Wave Breakup

A well-known effect of I_{to} is to promote a so-called spike-and-dome AP morphology. As the maximum conductance of I_{to} increases (58, 74), APD initially increases but then suddenly decreases once the maximum conductance reaches a certain value. This same effect can exhibit a large effect on APD restitution properties as shown in computer simulations (58) and experiments (59, 75). However, as shown in our recent studies (57, 58), I_{to} unmasks/exacerbates the effects of memory, resulting in a strong dependence of the APD restitution properties on the prior pacing history. Because of the memory effects, the slope of the APD restitution curve is not a good predictor of the APD instability, and memory has to be taken into account. Instead of calculating the APD restitution curves, we carried out simulations to show dynamical instabilities promoted by I_{to} in single cells (Figs. 3 and 8).

Based on our simulations of the LR1 model, I_{to} is not required for spiral wave breakup, and increasing the maximum I_{to} conductance can stabilize the spiral wave. Speeding up the $I_{Ca,L}$ kinetics flattens the APD restitution curve and stabilizes the spiral wave. However, under this condition, spiral wave breakup can be promoted by increasing the maximum I_{to} conductance. This insight can explain why the spiral waves are stable but breakup is promoted by I_{to} in tissue using the second-generation AP models. In other words, the fast $I_{Ca,L}$ kinetics results in stable spiral waves, but I_{to} promotes instabilities to cause spiral wave breakup. As shown in our simulations of the AP models, in the absence of I_{to}, it becomes difficult to promote spiral wave breakup by altering the maximum conductance of the other ionic currents, indicating a distinct role of I_{to} in promoting spiral wave instabilities. Note that I_{to} exhibits a fast and a slow component (abbreviated as $I_{to,f}$ and $I_{to,s}$, respectively). In our simulations, only the effect of $I_{to,f}$ (even though they are denoted as I_{to} in the AP models) was investigated. However, since $I_{to,s}$ recovers very slowly with a time constant $\sim$3 s (76), it remains mostly inactivated when the heart rate is fast. Therefore, it may not exhibit a large effect for spiral wave stability because the spiral wave CL ($<$300 ms) is much shorter than the recovery time of $I_{to,s}$. Moreover, besides its maximum conductance, the activation and inactivation kinetics of $I_{to,f}$ and its recovery time may still play an important role in spiral wave stability because the spiral wave CL is short.

We are not aware of any direct experiments demonstrating the role of I_{to} in spiral wave stability. In one experimental study (77), 4-AP, a selective blocker of I_{to}, converted VF to VT. This may agree with our simulation results suggesting that increasing I_{to} conductance promotes spiral wave breakup (e.g., VT to VF) and blocking I_{to} stabilizes spiral waves (VF to VT). In the optical mapping experiments of arrhythmias in Brugada syndrome by Aiba et al. (75), they observed VT and VF in different animals, and VT occurred in the ones with shortened APD and flattened APD restitution curves. This can be explained by the fact that a stronger I_{to} shortens APD and stabilizes spiral wave reentry as seen in our simulations.

Potential Caveats in the AP Models

As shown in previous simulations (44–47) and the current study, many of the second-generation AP models (48–52) give rise to stable spiral waves in a homogeneous tissue. Considering the experimental observations that spiral waves are unstable in normal undiseased hearts, one may assume that spiral wave breakup should occur in these AP models if the unstable spiral wave behaviors are caused by dynamical instabilities. This disagreement might lead one to argue that there are potential caveats in these AP models that prevent spiral wave breakup. One potential caveat is that too little I_{to} was included in these models and spiral wave breakup is caused by I_{to} in the real hearts. Although I_{to} may be present in many species (78), some species may not exhibit much I_{to}. For example, there is little I_{to} in the guinea pig ventricles (79). With no or a small I_{to}, the spiral wave is stable in the LRd guinea pig ventricular model, disagreeing with the experimental observations that spiral waves are unstable in guinea pig hearts. As we discussed above, stabilization of the spiral waves is due to the fast kinetics of $I_{Ca,L}$ in the models that have incorporated better patch-clamp experimental data. On the other hand, the recovery of $I_{Ca,L}$ of the Mahajan et al. model, the Hund and Rudy model, and 2006 ten Tusscher et al. model were slowed, spiral wave breakup then occurs in these models (44, 55, 71). Therefore, we argue that I_{to} may play a key role in spiral wave breakup in certain species and the recovery kinetics of $I_{Ca,L}$ in some of the AP models might need to be slowed to allow spiral wave breakup.

Limitations

Several limitations of the current study need to be mentioned. The maximum I_{to} conductance needed for spiral wave breakup or stabilizing the spiral wave is different for different AP models. For example, the maximum I_{to} conductance needed for spiral wave breakup in the LRd model and the Mahajan et al. model is roughly in the physiological range [see the literature survey in Nguyen et al. (78)]. However, the maximum I_{to} conductance needed for spiral wave breakup and stabilization in the TP04 model and the ORd model is very large. The difference may attribute to the different mathematical formulations of the AP models, which could be caveats in the AP models, as we discussed in the last section in DISCUSSION. On the other hand, there are other transient outward currents such as the small conductance Ca^{2+}-activated K^+ current (80, 81) and the Ca^{2+}-activated chloride current (82, 83). These currents may work in synergy with I_{to} to affect spiral wave stability.

In our simulations, we altered the maximum conductance of other ionic currents in the absence of I_{to} to investigate their contributions to spiral wave stability. Our conclusions may be biased due to the limited number of simulations and the choice of parameter ranges. Ideally, one may perform a parameter sensitivity analysis (84–87) to reveal the differential contribution of each ionic current to spiral wave stability, but due to the extremely high computational demand of tissue simulations, it is unrealistic to carry out the large number of simulations needed for regression analyses.

Unstable spiral wave dynamics observed in the real hearts can also be caused by spontaneous Ca^{2+} release. However, all AP models simulated in this study lack spontaneous Ca^{2+}

release, whose role in spiral wave breakup needs to be modeled using more detailed cell models (88) and multiscale computational methods (89).

Finally, we did not alter the $I_{Ca,L}$ recovery properties of other models but the activation and inactivation time constants of I_{si} in the LR1 model to investigate the role of $I_{Ca,L}$ recovery on spiral wave stability. However, changing both time constants changes not only the recovery but also other properties, such as the conductance of $I_{Ca,L}$, and thus the stabilization of the spiral wave may not only be attributed to I_{si} recovery. As we mentioned in detail in the section of the LR1 model in RESULTS, one of the major improvements of the second-generation AP models is the speedup of the $I_{Ca,L}$ kinetics, which results in stable spiral waves for these models. On the other hand, spiral wave stability in a homogeneous tissue is a dynamical property that can be affected by many parameters (maximum conductance, time constants, and ion concentrations, etc.), and parameter sensitivity analyses may be needed to pinpoint the differential contributions of the parameters. Nevertheless, based on the previous studies, $I_{Ca,L}$ recovery is a key parameter for spiral wave stability and our findings show that I_{to} conductance is another key parameter for spiral wave stability in cardiac tissue.

Conclusions

Besides $I_{Ca,L}$ recovery kinetics, the maximum I_{to} conductance is another key parameter that can promote spiral wave breakup in cardiac tissue. It may contribute to the unstable spiral wave dynamics observed in experiments of normal hearts and may play important roles in promoting the transition from VT to VF in Brugada syndrome.

GRANTS

This study was supported by National Institutes of Health Grants R01 HL139829, R01 HL134709, and F30 HL140864; Zhejiang Province Commonweal Projects Grant LGF18A050001 (to X.Y.); and China Scholarship Council Grant No. 201708330401 (to X.Y.).

DISCLOSURES

No conflicts of interest, financial or otherwise, are declared by the authors.

AUTHOR CONTRIBUTIONS

J.L., P-S.C., and Z.Q. conceived and designed research; J.L. and X.Y. performed experiments; J.L. and Z.Q. analyzed data; J.L., X.Y., and Z.Q. prepared figures; J.L. and Z.Q. drafted manuscript; J.L., P-S.C., and Z.Q. edited and revised manuscript; J.L., X.Y., P-S.C., and Z.Q. approved final version of manuscript.

REFERENCES

1. **Zipes DP**, **Wellens HJ.** Sudden cardiac death. *Circulation* 98: 2334–2351, 1998. doi:10.1161/01.CIR.98.21.2334.
2. **Qu Z**, **Weiss JN.** Mechanisms of ventricular arrhythmias: from molecular fluctuations to electrical turbulence. *Annu Rev Physiol* 77: 29–55, 2015. doi:10.1146/annurev-physiol-021014-071622.
3. **Rosen MR.** Mechanisms for arrhythmias. *Am J Cardiol* 61: 2A–8A, 1988. doi:10.1016/0002-9149(88)90735-7.
4. **Aras KK**, **Kay MW**, **Efimov IR.** Ventricular fibrillation: rotors or foci? Both! *Circ Arrhythm Electrophysiol* 10: e006011, 2017. doi:10.1161/CIRCEP.117.006011.
5. **Choi BR**, **Liu T**, **Salama G.** Ventricular fibrillation: mother rotor or multiple wavelets? *Circ Res* 89: E30, 2001.
6. **Ideker RE**, **Rogers JM.** Human ventricular fibrillation: wandering wavelets, mother rotors, or both? *Circulation* 114: 530–532, 2006. doi:10.1161/CIRCULATIONAHA.106.644765.
7. **Janse MJ.** Focus, reentry, or "focal" reentry? *Am J Physiol Heart Circ Physiol* 292: H2561–H2562, 2007. doi:10.1152/ajpheart.00167.2007.
8. **Chen J**, **Mandapati R**, **Berenfeld O**, **Skanes AC**, **Jalife J.** High-frequency periodic sources underlie ventricular fibrillation in the isolated rabbit heart. *Circ Res* 86: 86–93, 2000. doi:10.1161/01.RES.86.1.86.
9. **Davidenko JM**, **Pertsov AM**, **Salomonsz R**, **Baxter W**, **Jalife J.** Stationary and drifting spiral waves of excitation in isolated cardiac muscle. *Nature* 355: 349–351, 1992. doi:10.1038/355349a0.
10. **Garfinkel A**, **Kim YH**, **Voroshilovsky O**, **Qu Z**, **Kil JR**, **Lee MH**, **Karagueuzian HS**, **Weiss JN**, **Chen PS.** Preventing ventricular fibrillation by flattening cardiac restitution. *Proc Natl Acad Sci USA* 97: 6061–6066, 2000. doi:10.1073/pnas.090492697.
11. **Gray RA**, **Jalife J**, **Panfilov AV**, **Baxter WT**, **Cabo C**, **Davidenko JM**, **Pertsov AM.** Nonstationary vortexlike reentrant activity as a mechanism of polymorphic ventricular tachycardia in the isolated rabbit heart. *Circulation* 91: 2454–2469, 1995. doi:10.1161/01.CIR.91.9.2454.
12. **Gray RA**, **Jalife J**, **Panfilov AV**, **Baxter WT**, **Cabo C**, **Davidenko JM**, **Pertsov AM**, **Winfree AT.** Mechanisms of cardiac fibrillation. *Science* 270: 1222–1225, 1995. doi:10.1126/science.270.5239.1222.
13. **Gray RA**, **Pertsov AM**, **Jalife J.** Spatial and temporal organization during cardiac fibrillation. *Nature (London)* 392: 75–78, 1998 [Erratum in *Nature* 393: 191, 1998]. doi:10.1038/32164.
14. **Kay MW**, **Walcott GP**, **Gladden JD**, **Melnick SB**, **Rogers JM.** Lifetimes of epicardial rotors in panoramic optical maps of fibrillating swine ventricles. *Am J Physiol Heart Circ Physiol* 291: H1935–H1941, 2006. doi:10.1152/ajpheart.00276.2006.
15. **Pandit SV**, **Warren M**, **Mironov S**, **Tolkacheva EG**, **Kalifa J**, **Berenfeld O**, **Jalife J.** Mechanisms underlying the antifibrillatory action of hyperkalemia in guinea pig hearts. *Biophys J* 98: 2091–2101, 2010. doi:10.1016/j.bpj.2010.02.011.
16. **Park SA**, **Gray RA.** Optical mapping of ventricular fibrillation dynamics. In: *Membrane Potential Imaging in the Nervous System and Heart*, edited by Canepari M, Zecevic D, Bernus O. Cham: Springer International Publishing, 2015, p. 313–342.
17. **Samie FH**, **Berenfeld O**, **Anumonwo J**, **Mironov SF**, **Udassi S**, **Beaumont J**, **Taffet S**, **Pertsov AM**, **Jalife J.** Rectification of the background potassium current - a determinant of rotor dynamics in ventricular fibrillation. *Circ Res* 89: 1216–1223, 2001. doi:10.1161/hh2401.100818.
18. **Valderrábano M**, **Yang J**, **Omichi C**, **Kil J**, **Lamp ST**, **Qu Z**, **Lin S-F**, **Karagueuzian HS**, **Garfinkel A**, **Chen P-S**, **Weiss JN.** Frequency analysis of ventricular fibrillation in swine ventricles. *Circ Res* 90: 213–222, 2002. doi:10.1161/hh0202.103645.
19. **Vandersickel N**, **Bossu A**, **De Neve J**, **Dunnink A**, **Meijborg VMF**, **van der Heyden MAG**, **Beekman JDM**, **De Bakker JMT**, **Vos MA**, **Panfilov AV.** Short-lasting episodes of torsade de pointes in the chronic atrioventricular block dog model have a focal mechanism, while longer-lasting episodes are maintained by re-entry. *JACC Clin Electrophysiol* 3: 1565–1576, 2017. doi:10.1016/j.jacep.2017.06.016.
20. **Warren M**, **Guha PK**, **Berenfeld O**, **Zaitsev A**, **Anumonwo JMB**, **Dhamoon AS**, **Bagwe S**, **Taffet SM**, **Jalife J.** Blockade of the inward rectifying potassium current terminates ventricular fibrillation in the guinea pig heart. *J Cardiovasc Electrophysiol* 14: 621–631, 2003. doi:10.1046/j.1540-8167.2003.03006.x.
21. **Wu TJ**, **Lin SF**, **Baher A**, **Qu Z**, **Garfinkel A**, **Weiss JN**, **Ting CT**, **Chen PS.** Mother rotors and the mechanisms of D600-induced type 2 ventricular fibrillation. *Circulation* 110: 2110–2118, 2004. doi:10.1161/01.CIR.0000143834.51102.91.
22. **Massé S**, **Downar E**, **Chauhan V**, **Sevaptsidis E**, **Nanthakumar K.** Ventricular fibrillation in myopathic human hearts: mechanistic insights from in vivo global endocardial and epicardial mapping. *Am J Physiol Heart Circ Physiol* 292: H2589–H2597, 2007. doi:10.1152/ajpheart.01336.2006.
23. **Nair K**, **Umapathy K**, **Farid T**, **Masse S**, **Mueller E**, **Sivanandan RV**, **Poku K**, **Rao V**, **Nair V**, **Butany J**, **Ideker RE**, **Nanthakumar K.**

Intramural activation during early human ventricular fibrillation. *Circ Arrhythm Electrophysiol* 4: 692–703, 2011. doi:10.1161/CIRCEP.110.961037.

24. **Nash MP**, **Mourad A**, **Clayton RH**, **Sutton PM**, **Bradley CP**, **Hayward M**, **Paterson DJ**, **Taggart P.** Evidence for multiple mechanisms in human ventricular fibrillation. *Circulation* 114: 536–542, 2006. doi:10.1161/CIRCULATIONAHA.105.602870.
25. **Choi BR**, **Nho W**, **Liu T**, **Salama G.** Life span of ventricular fibrillation frequencies. *Circ Res* 91: 339–345, 2002. doi:10.1161/01.RES.0000031801.84308.F4.
26. **Weiss JN**, **Chen PS**, **Qu Z**, **Karagueuzian HS**, **Garfinkel A.** Ventricular fibrillation: how do we stop the waves from breaking? *Circ Res* 87: 1103–1107, 2000. doi:10.1161/01.RES.87.12.1103.
27. **Karma A.** Electrical alternans and spiral wave breakup in cardiac tissue. *Chaos* 4: 461–472, 1994. doi:10.1063/1.166024.
28. **Karma A.** Spiral breakup in model equations of action potential propagation in cardiac tissue. *Phys Rev Lett* 71: 1103–1106, 1993. doi:10.1103/PhysRevLett.71.1103.
29. **Courtemanche M.** Complex spiral wave dynamics in a spatially distributed ionic model of cardiac electrical activity. *Chaos* 6: 579–600, 1996. doi:10.1063/1.166206.
30. **Courtemanche M**, **Winfree AT.** Re-entrant rotating waves in a Beeler-Reuter based model of two-dimensional cardiac conduction. *Int J Bifurcation Chaos* 01: 431–444, 1991. doi:10.1142/S0218127491000336.
31. **Fenton F**, **Karma A.** Vortex dynamics in three-dimensional continuous myocardium with fiber rotation: filament instability and fibrillation. *Chaos* 8: 20–47, 1998. doi:10.1063/1.166311.
32. **Leon LJ**, **Roberge FA**, **Vinet A.** Simulation of two-dimensional anisotropic cardiac reentry: effects of the wavelength on the reentry characteristics. *Ann Biomed Eng* 22: 592–609, 1994. doi:10.1007/BF02368286.
33. **Qu Z**, **Weiss JN**, **Garfinkel A.** Cardiac electrical restitution properties and the stability of reentrant spiral waves: a simulation study. *Am J Physiol* 276: H269–H283, 1999. doi:10.1152/ajpheart.1999.276.1.H269.
34. **Bernus O**, **Wilders R**, **Zemlin CW**, **Verschelde H**, **Panfilov AV.** A computationally efficient electrophysiological model of human ventricular cells. *Am J Physiol Heart Circ Physiol* 282: H2296–H2308, 2002. doi:10.1152/ajpheart.00731.2001.
35. **Fenton FH**, **Cherry EM**, **Hastings HM**, **Evans SJ.** Multiple mechanisms of spiral wave breakup in a model of cardiac electrical activity. *Chaos* 12: 852–892, 2002. doi:10.1063/1.1504242.
36. **Panfilov A**, **Pertsov A.** Ventricular fibrillation: evolution of the multiple-wavelet hypothesis. *Philos Trans A Math Phys Eng Sci* 359: 1315–1325, 2001. doi:10.1098/rsta.2001.0833.
37. **Panfilov AV.** Spiral breakup as a model of ventricular fibrillation. *Chaos* 8: 57–64, 1998. doi:10.1063/1.166287.
38. **Qu Z**, **Xie F**, **Garfinkel A**, **Weiss JN.** Origins of spiral wave meander and breakup in a two-dimensional cardiac tissue model. *Ann Biomed Eng* 28: 755–771, 2000. doi:10.1114/1.1289474.
39. **Banville I**, **Gray RA.** Effect of action potential duration and conduction velocity restitution and their spatial dispersion on alternans and the stability of arrhythmias. *J Cardiovasc Electrophysiol* 13: 1141–1149, 2002. doi:10.1046/j.1540-8167.2002.01141.x.
40. **Koller ML**, **Riccio ML**, **Gilmour RF, Jr.** Dynamic restitution of action potential duration during electrical alternans and ventricular fibrillation. *Am J Physiol* 275: H1635–H1642, 1998. doi:10.1152/ajpheart.1998.275.5.H1635.
41. **Lee MH**, **Lin SF**, **Ohara T**, **Omichi C**, **Okuyama Y**, **Chudin E**, **Garfinkel A**, **Weiss JN**, **Karagueuzian HS**, **Chen PS.** Effects of diacetyl monoxime and cytochalasin D on ventricular fibrillation in swine right ventricles. *Am J Physiol Heart Circ Physiol* 280: H2689–H2696, 2001. doi:10.1152/ajpheart.2001.280.6.H2689.
42. **Lou Q**, **Li W**, **Efimov IR.** The role of dynamic instability and wavelength in arrhythmia maintenance as revealed by panoramic imaging with blebbistatin vs. 2,3-butanedione monoxime. *Am J Physiol Heart Circ Physiol* 302: H262–H269, 2012. doi:10.1152/ajpheart.00711.2011.
43. **Wu TJ**, **Lin SF**, **Weiss JN**, **Ting CT**, **Chen PS.** Two types of ventricular fibrillation in isolated rabbit hearts - Importance of excitability and action potential duration restitution. *Circulation* 106: 1859–1866, 2002. doi:10.1161/01.CIR.0000031334.49170.FB.
44. **Cherry EM**, **Fenton FH.** A tale of two dogs: analyzing two models of canine ventricular electrophysiology. *Am J Physiol Heart Circ Physiol* 292: H43–H55, 2007. doi:10.1152/ajpheart.00955.2006.
45. **Cherry EM**, **Fenton FH.** Visualization of spiral and scroll waves in simulated and experimental cardiac tissue. *New J Phys* 10: 125016, 2008. doi:10.1088/1367-2630/10/12/125016.
46. **Elshrif MM**, **Cherry EM.** A quantitative comparison of the behavior of human ventricular cardiac electrophysiology models in tissue. *PLoS One* 9: e84401, 2014. doi:10.1371/journal.pone.0084401.
47. **Shajahan TK**, **Nayak AR**, **Pandit R.** Spiral-wave turbulence and its control in the presence of inhomogeneities in four mathematical models of cardiac tissue. *PLOS One* 4: e4738, 2009. doi:10.1371/journal.pone.0004738.
48. **Grandi E**, **Pasqualini FS**, **Bers DM.** A novel computational model of the human ventricular action potential and Ca transient. *J Mol Cell Cardiol* 48: 112–121, 2010. doi:10.1016/j.yjmcc.2009.09.019.
49. **Luo CH**, **Rudy Y.** A dynamical model of the cardiac ventricular action potential: I. simulations of ionic currents and concentration changes. *Circ Res* 74: 1071–1096, 1994. doi:10.1161/01.RES.74.6.1071.
50. **O'Hara T**, **Virag L**, **Varro A**, **Rudy Y.** Simulation of the undiseased human cardiac ventricular action potential: model formulation and experimental validation. *PLoS Comput Biol* 7: e1002061, 2011. doi:10.1371/journal.pcbi.1002061.
51. **Priebe L**, **Beuckelmann DJ.** Simulation study of cellular electric properties in heart failure. *Circ Res* 82: 1206–1223, 1998. doi:10.1161/01.RES.82.11.1206.
52. **ten Tusscher KH**, **Noble D**, **Noble PJ**, **Panfilov AV.** A model for human ventricular tissue. *Am J Physiol Heart Circ Physiol* 286: H1573–H1589, 2004. doi:10.1152/ajpheart.00794.2003.
53. **Hund TJ**, **Rudy Y.** Rate dependence and regulation of action potential and calcium transient in a canine cardiac ventricular cell model. *Circulation* 110: 3168–3174, 2004. doi:10.1161/01.CIR.0000147231.69595.D3.
54. **Iyer V**, **Mazhari R**, **Winslow RL.** A computational model of the human left-ventricular epicardial myocyte. *Biophys J* 87: 1507–1525, 2004. doi:10.1529/biophysj.104.043299.
55. **ten Tusscher KH**, **Panfilov AV.** Alternans and spiral breakup in a human ventricular tissue model. *Am J Physiol Heart Circ Physiol* 291: H1088–H1100, 2006. doi:10.1152/ajpheart.00109.2006.
56. **Hopenfeld B.** Mechanism for action potential alternans: the interplay between L-type calcium current and transient outward current. *Heart Rhythm* 3: 345–352, 2006. doi:10.1016/j.hrthm.2005.11.016.
57. **Landaw J**, **Garfinkel A**, **Weiss JN**, **Qu Z.** Memory-induced chaos in cardiac excitation. *Phys Rev Lett* 118: 138101, 2017. doi:10.1103/PhysRevLett.118.138101.
58. **Landaw J**, **Qu Z.** Memory-induced nonlinear dynamics of excitation in cardiac diseases. *Phys Rev E* 97: 042414, 2018. doi:10.1103/PhysRevE.97.042414.
59. **Lukas A**, **Antzelevitch C.** Differences in the electrophysiological response of canine ventricular epicardium and endocardium to ischemia. Role of the transient outward current. *Circulation* 88: 2903–2915, 1993. doi:10.1161/01.CIR.88.6.2903.
60. **Brahmajothi MV**, **Campbell DL**, **Rasmusson RL**, **Morales MJ**, **Trimmer JS**, **Nerbonne JM**, **Strauss HC.** Distinct transient outward potassium current (I_{to}) phenotypes and distribution of fast-inactivating potassium channel alpha subunits in ferret left ventricular myocytes. *J Gen Physiol* 113: 581–600, 1999. doi:10.1085/jgp.113.4.581.
61. **NäBauer M**, **Beuckelmann DJ**, **ÛBerfuhr P**, **Steinbeck G.** Regional differences in current density and rate-dependent properties of the transient outward current in subepicardial and subendocardial myocytes of human left ventricle. *Circulation* 93: 168–177, 1996. doi:10.1161/01.CIR.93.1.168.
62. **Antzelevitch C**, **Yan G-X.** J-wave syndromes: Brugada and early repolarization syndromes. *Heart Rhythm* 12: 1852–1866, 2015. doi:10.1016/j.hrthm.2015.04.014.
63. **Antzelevitch C**, **Yan G-X**, **Ackerman MJ**, **Borggrefe M**, **Corrado D**, **Guo J**, **Gussak I**, **Hasdemir C**, **Horie M**, **Huikuri H**, **Ma C**, **Morita H**, **Nam G-B**, **Sacher F**, **Shimizu W**, **Viskin S**, **Wilde AAM.** J-Wave syndromes expert consensus conference report: Emerging concepts and gaps in knowledge. *Heart Rhythm* 13: e295–e324, 2016. doi:10.1016/j.hrthm.2016.05.024.
64. **Lukas A**, **Antzelevitch C.** Phase 2 reentry as a mechanism of initiation of circus movement reentry in canine epicardium exposed to

simulated ischemia. *Cardiovasc Res* 32: 593–603, 1996. doi:10.1016/S0008-6363(96)00115-0.
65. **Maoz A**, **Christini DJ**, **Krogh-Madsen T.** Dependence of phase-2 reentry and repolarization dispersion on epicardial and transmural ionic heterogeneity: a simulation study. *Europace* 16: 458–465, 2014. doi:10.1093/europace/eut379.
66. **Luo CH**, **Rudy Y.** A model of the ventricular cardiac action potential: depolarization, repolarization, and their interaction. *Circ Res* 68: 1501–1526, 1991. doi:10.1161/01.RES.68.6.1501.
67. **Faber GM**, **Rudy Y.** Action potential and contractility changes in [Na(+)](i) overloaded cardiac myocytes: a simulation study. *Biophys J* 78: 2392–2404, 2000. doi:10.1016/S0006-3495(00)76783-X.
68. **Mahajan A**, **Shiferaw Y**, **Sato D**, **Baher A**, **Olcese R**, **Xie L-H**, **Yang M-J**, **Chen P-S**, **Restrepo JG**, **Karma A**, **Garfinkel A**, **Qu Z**, **Weiss JN.** A rabbit ventricular action potential model replicating cardiac dynamics at rapid heart rates. *Biophys J* 94: 392–410, 2008. doi:10.1529/biophysj.106.98160.
69. **Gima K**, **Rudy Y.** Ionic current basis of electrocardiographic waveforms: a model study. *Circ Res* 90: 889–896, 2002. doi:10.1161/01.RES.0000016960.61087.86.
70. **Beeler GW**, **Reuter H.** Reconstruction of the action potential of ventricular myocardial fibres. *J Physiol* 268: 177–210, 1977. doi:10.1113/jphysiol.1977.sp011853.
71. **Mahajan A**, **Sato D**, **Shiferaw Y**, **Baher A**, **Xie L-H**, **Peralta R**, **Olcese R**, **Garfinkel A**, **Qu Z**, **Weiss JN.** Modifying L-type calcium current kinetics: consequences for cardiac excitation and arrhythmia dynamics. *Biophys J* 94: 411–423, 2008. doi:10.1529/biophysj.106.98590.
72. **Qu Z.** Dynamical effects of diffusive cell coupling on cardiac excitation and propagation: a simulation study. *Am J Physiol Heart Circ Physiol* 287: H2803–H2812, 2004. doi:10.1152/ajpheart.00299.2004.
73. **Xie F**, **Qu Z**, **Garfinkel A**, **Weiss JN.** Electrophysiological heterogeneity and stability of reentry in simulated cardiac tissue. *Am J Physiol Heart Circ Physiol* 280: H535–H545, 2001. doi:10.1152/ajpheart.2001.280.2.H535.
74. **Greenstein JL**, **Wu R**, **Po S**, **Tomaselli GF**, **Winslow RL.** Role of the calcium-independent transient outward current I(to1) in shaping action potential morphology and duration. *Circ Res* 87: 1026–1033, 2000. doi:10.1161/01.RES.87.11.1026.
75. **Aiba T**, **Shimizu W**, **Hidaka I**, **Uemura K**, **Noda T**, **Zheng C**, **Kamiya A**, **Inagaki M**, **Sugimachi M**, **Sunagawa K.** Cellular basis for trigger and maintenance of ventricular fibrillation in the brugada syndrome model: high-resolution optical mapping study. *J Am Coll Cardiol* 47: 2074–2085, 2006. doi:10.1016/j.jacc.2005.12.064.
76. **Bassani RA**, **Altamirano J**, **Puglisi JL**, **Bers DM.** Action potential duration determines sarcoplasmic reticulum Ca2+ reloading in mammalian ventricular myocytes. *J Physiol* 559: 593–609, 2004. doi:10.1113/jphysiol.2004.067959.
77. **Miyashita T**, **Kubota I**, **Yamaki M**, **Watanabe T**, **Yamauchi S**, **Tomoike H.** 4-aminopyridine inhibits the occurrence of ventricular fibrillation but not ventricular tachycardia in the reperfused, isolated rat heart. *Jpn Circ J* 64: 602–605, 2000. doi:10.1253/jcj.64.602.
78. **Nguyen TP**, **Singh N**, **Xie Y**, **Qu Z**, **Weiss JN.** Repolarization reserve evolves dynamically during the cardiac action potential: effects of transient outward currents on early afterdepolarizations. *Circ Arrhythm Electrophysiol* 8: 694–702, 2015. doi:10.1161/CIRCEP.114.002451.
79. **Sicouri S**, **Quist M**, **Antzelevitch C.** Evidence for the presence of M cells in the guinea pig ventricle. *J Cardiovasc Electrophysiol* 7: 503–511, 1996. doi:10.1111/j.1540-8167.1996.tb00557.x.
80. **Hamilton S**, **Polina I**, **Terentyeva R**, **Bronk P**, **Kim TY**, **Roder K**, **Clements RT**, **Koren G**, **Choi B-R**, **Terentyev D.** PKA phosphorylation underlies functional recruitment of sarcolemmal SK2 channels in ventricular myocytes from hypertrophic hearts. *J Physiol* 598: 2847–2873, 2020. doi:10.1113/JP277618.
81. **Landaw J**, **Zhang Z**, **Song Z**, **Liu MB**, **Olcese R**, **Chen P-S**, **Weiss JN**, **Qu Z.** Small-conductance Ca2+-activated K+ channels promote J-wave syndrome and phase 2 reentry. *Heart Rhythm* 17: 1582–1590, 2020. doi:10.1016/j.hrthm.2020.04.023.
82. **Hegyi B**, **Bossuyt J**, **Griffiths LG**, **Shimkunas R**, **Coulibaly Z**, **Jian Z**, **Grimsrud KN**, **Sondergaard CS**, **Ginsburg KS**, **Chiamvimonvat N**, **Belardinelli L**, **Varró A**, **Papp JG**, **Pollesello P**, **Levijoki J**, **Izu LT**, **Boyd WD**, **Bányász T**, **Bers DM**, **Chen-Izu Y.** Complex electrophysiological remodeling in postinfarction ischemic heart failure. *Proc Natl Acad Sci USA* 115: E3036–E3044, 2018. doi:10.1073/pnas.1718211115.
83. **Verkerk AO**, **Veldkamp MW**, **Baartscheer A**, **Schumacher CA**, **Klöpping C**, **van Ginneken AC**, **Ravesloot JH.** Ionic mechanism of delayed after depolarizations in ventricular cells isolated from human end-stage failing hearts. *Circulation* 104: 2728–2733, 2001. doi:10.1161/hc4701.099577.
84. **Morotti S**, **Grandi E.** Logistic regression analysis of populations of electrophysiological models to assess proarrythmic risk. *MethodsX* 4: 25–34, 2017. doi:10.1016/j.mex.2016.12.002.
85. **Passini E**, **Mincholé A**, **Coppini R**, **Cerbai E**, **Rodriguez B**, **Severi S**, **Bueno-Orovio A.** Mechanisms of pro-arrhythmic abnormalities in ventricular repolarisation and anti-arrhythmic therapies in human hypertrophic cardiomyopathy. *J Mol Cell Cardiol* 96: 72–81, 2016. doi:10.1016/j.yjmcc.2015.09.003.
86. **Sarkar AX**, **Sobie EA.** Regression analysis for constraining free parameters in electrophysiological models of cardiac cells. *PLoS Comput Biol* 6: e1000914, 2010. doi:10.1371/journal.pcbi.1000914.
87. **Sobie EA.** Parameter sensitivity analysis in electrophysiological models using multivariable regression. *Biophys J* 96: 1264–1274, 2009. doi:10.1016/j.bpj.2008.10.056.
88. **Song Z**, **Ko CY**, **Nivala M**, **Weiss JN**, **Qu Z.** Calcium-voltage coupling in the genesis of early and delayed after depolarizations in cardiac myocytes. *Biophys J* 108: 1908–1921, 2015. doi:10.1016/j.bpj.2015.03.011.
89. **Colman MA.** Arrhythmia mechanisms and spontaneous calcium release: bi-directional coupling between re-entrant and focal excitation. *PLOS Comput Biol* 15: e1007260, 2019. doi:10.1371/journal.pcbi.1007260.